Analysis of Damage due to the M6.4 Tuban-Bawean Earthquake using Remote Sensing

Siti Asmayanti Tuasamu[1], *Mokhamad Nur* Cahyadi[1*], *Nilam* Komalasari[1], *Candida Aulia De Silva* Nusantara[1], *Amien* Widodo[2], *Nurrohmat* Widjajanti[3], *Evi* Aprianti[4], *Deni* Kusumawardani[5], *Yessi* Rahmawati[5], and *Iqbal Hanun* Azizi[3]

[1] Department of Geomatics Engineering, Faculty of Civil, Planning, and Earth Engineering, Institut Teknologi Sepuluh Nopember, Surabaya, Indonesia
[2] Department Geophysical Engineering, Faculty of Civil, Planning, and Earth Engineering, Institut Teknologi Sepuluh Nopember, Surabaya, Indonesia
[3] Department Geodetic Engineering, Universitas Gadjah Mada,Yogyakarta, Indonesia
[4] Department Disaster Management Universitas Hasanuddin, Indonesia
[5] Department Economic Development, Universitas Airlangga, Indonesia

Abstract. The earthquake with magnitude 6.4 that occurred on March 22, 2024 in Tuban-Bawean, East Java, Indonesia, had a significant impact on infrastructure damage around the Tuban, Gresik, Tuban, and Surabaya Islands. By combining geophysical analysis, the Okada model, and remote sensing technology, this study seeks to examine the effects following an earthquake. A comparatively slight variance is indicated by the deformation of land movement surrounding Bawean Island, which ranges from -0.0091 to 0.0069 meters, indicating relatively small variation. This is consistent with the results of the Okada modeling showing minimal vertical movement which is a characteristic of strike-slip faults. The majority of the affected areas, namely Sangkapura District, are dominated by alluvial lithology (Qa), which is very vulnerable to the impact of earthquakes because the material is loose, loose, and unconsolidated. Thus strengthening the effects of earthquake shocks and causing more significant damage. On the other hand, volcanic rocks (Qv) composed of alternating lava, breccia and tuff tend to experience greater deformation because they are easily affected by tectonic forces. This study concludes that the integration of remote sensing techniques, Okada modeling, and geophysical analysis provides a comprehensive understanding for post-earthquake analysis. It is hoped that this study can contribute to disaster mitigation efforts in the future.

1 Introduction

Earthquake disaster mitigation studies can be carried out by utilizing GNSS (Global Navigation Satellite System) technology. Determining the position of a particular point on the earth's surface can be done accurately using the GNSS system. Currently, GNSS technology has developed very rapidly. The GNSS technology has been widely used in

*Corresponding author: cahyadi@geodesy.its.ac.id

various applications nowadays such as ionosphere studies for earthquakes [1-4], tsunamis [5-6], volcanic eruptions [7-8], and land subsidence monitoring [9].

The Tuban-Bawean region has experienced a series of significant earthquakes as shown in Table 1. On March 22, 2024, there is a series of earthquakes occurred in the Tuban-Bawean region [10]. The first series of earthquakes with a magnitude of M 5.6 occurred at 04:22:54 UTC with a depth of 10 km. Furthermore, the second earthquake with a magnitude of M 5.2 occurred at 05:31:12 UTC with a depth of 10 km. The third earthquake was an earthquake with a magnitude of M 6.4 greater than the first and second earthquakes which occurred at 08:52:58 UTC with a depth of 9.5 km which can be seen in Figure 1. This earthquake with a magnitude of M 6.4 was the cause of infrastructure and environmental damage on Bawean Island, Gresik, Tuban and Surabaya.

Table 1. Earthquake history in Tuban-Bawean [10].

Magnitude	Depth	Epicenter	Time (UTC)
M 5.6 - 117 km N of Paciran, Indonesia	10 km	5.816°S 112.319°E	2024-03-22 04:22:45
M 5.2 - 107 km N of Paciran, Indonesia	10 km	5.909°S 112.383°E10.0	2024-03-22 05:31:12
M 6.4 - 110 km N of Paciran, Indonesia	**9.5 km**	**5.909°S 112.383°E**	**2024-03-22 08:52:58**
M 4.7 - 111 km N of Paciran, Indonesia	10 km	5.869°S 112.459°E	2024-03-22 09:19:27
M 4.6 - 110 km N of Paciran, Indonesia	10 km	5.880°S 112.401°E	2024-03-22 09:55:46
M 4.5 - 117 km N of Paciran, Indonesia	10 km	5.817°S 112.364°E	2024-03-22 10:57:22
M 4.5 - 110 km N of Paciran, Indonesia	10 km	5.881°S 112.391°E	2024-03-22 21:42:01
M 4.2 - 120 km N of Paciran, Indonesia	10.2 km	5.791°S 112.382°E	2024-03-25 21:05:52
M 4.4 - 110 km N of Paciran, Indonesia	17.4 km	5.884°S 112.480°E	2024-03-28 21:23:02
M 4.2 - 124 km NNE of Paciran, Indonesia	10 km	5.770°S 112.604°E	2024-03-30 21:43:19
M 4.1 - 125 km NNE of Paciran, Indonesia	12 km	5.771°S 112.636°E	2024-04-01 10:26:27
M 5.1 - 111 km N of Paciran, Indonesia	10 km	5.865°S 112.339°E	2024-04-03 09:02:16
M 4.4 - 118 km N of Paciran, Indonesia	9.7 km	5.819°S 112.514°E	2024-04-11 23:14:35
M 4.6 - 120 km N of Paciran, Indonesia	10 km	5.785°S 112.353°E	2024-04-17 08:15:05
M 4.2 - 117 km N of Paciran, Indonesia	10 km	5.820°S 112.496°E	2024-05-12 14:33:05
M 4.8 - 120 km N of Paciran, Indonesia	10 km	5.801°S 112.521°E	2024-05-13 06:42:29

Conventional earthquake impact analysis through field surveys has limitations such as spatial coverage and the time required. It is also limited to remote or hard-to-reach areas. Nowadays, remote sensing technology has evolved into an analytical tool for mapping earthquake impacts in a wide scale and high resolution [11-12]. When it comes to analyzing ground movement caused by seismic activity such as earthquakes, geophysical models such as the Okada model are often used [13]. This model allows simulation of earth surface deformation based on earthquake parameters such as dip, strike and slip, so as to estimate the distribution of ground shifts around the earthquake zone [14-16].

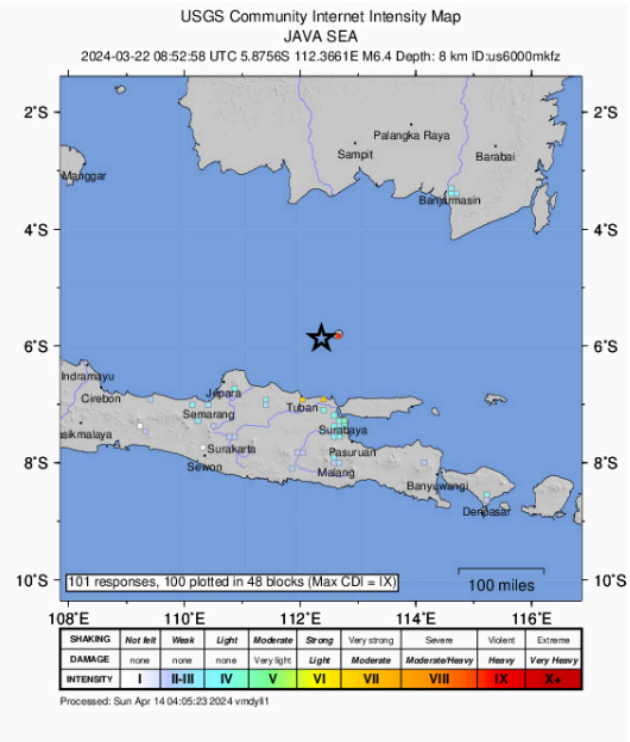

Fig. 1. Location map of the M6.4 Tuban-Bawean earthquake. The black star shows the epicentre of the earthquake and the red dot near the epicentre is Bawean Island [10].

This research looks at combining remote sensing methods with Okada modeling to study earthquakes in the Bawean Island area. We will use satellite images and apply remote sensing techniques to analyze land deformation. At the same time, we will use Okada modeling to forecast ground movement based on the earthquake details. Investigation of the relationship between land movement and lithological conditions in the Bawean Island area, especially the presence of alluvial deposits (Qa) will also be conducted to strengthen the research results. Through an integrated approach of remote sensing technology, Okada modeling, and local geological analysis, it is hoped that this research can analyze the impact of earthquakes more comprehensively and contribute to earthquake disaster mitigation efforts.

2 Methodology

This research location is an earthquake area, which is located between 5°43' and 5°52' N and 112°34' and 112°44' East. The main focus of this research is the analysis of Bawean Island, Gresik Regency, East Java Province as the affected area of the M 6.4 Tuban-Bawean earthquake, especially Sangkapura sub-district.

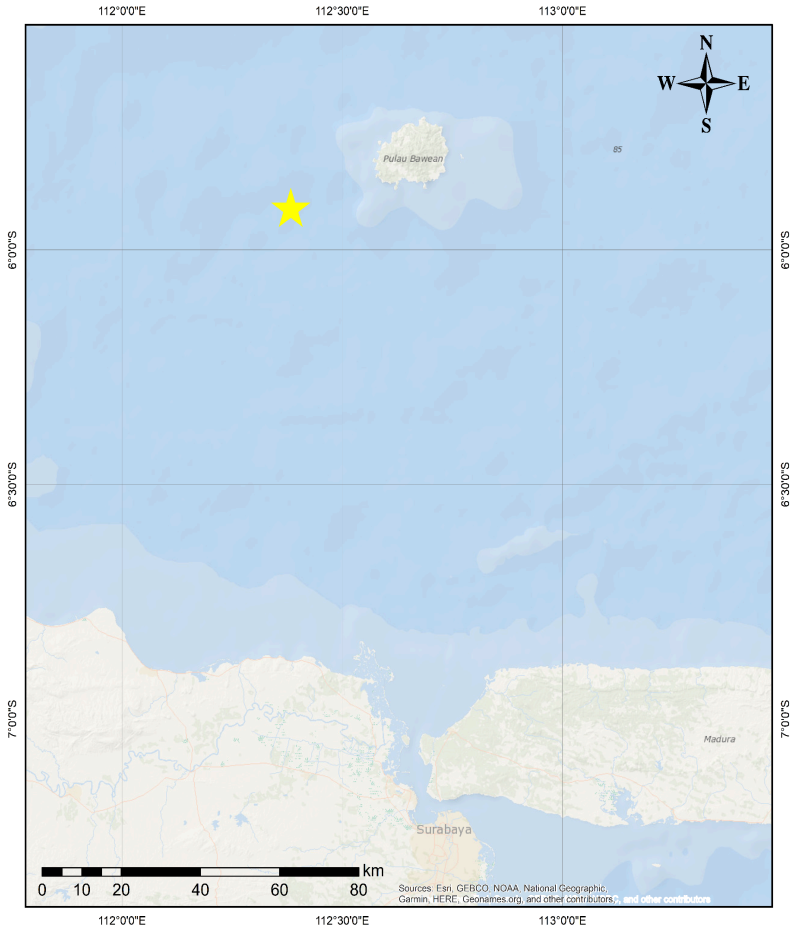

Fig. 2. Location map of Bawean island. Yellow star shows the epicentre of the earthquake.

In this study, an integration of remote sensing methods and the Okada model was carried out to analyze the damage caused by the M6.4 earthquake in Tuban-Bawean which occurred on March 22, 2024. This earthquake was an earthquake with a focal strike-slip mechanism. The primary data used in this study are two Sentinel-1A SAR images (level 1.0) on March 14, 2024 and March 26, 2024. In addition, the Digital Elevation Model (DEM) SRTM 3 at the research location was also used.

Table 2. Metadata citra Sentinel 1A.

ID Scene	Date	Direction	Usability

S1A_IW_SLC__1SDV_20240314T105049_20240314T105115_052976_0669B7_ACEF	March 14, 2024	Descending	Master
S1A_IW_SLC__1SDV_20240326T105049_20240326T105115_053151_067077_6764	March 26, 2024	Descending	Slave

The first process is the formation of the Single Look Complex (SLC), which is done so that the image is radiometrically calibrated at the sensor input, given that the Sentinel-1A image has an array of uncompressed signal data and requires geometric correction. SAR Processing includes SAR parameter reading, Radar Signal Processing, and range and azimuth compression. Next, Interferometry SAR Processing is performed to form an interferogram image from a pair of SLC data. The resulting raw interferogram is a phase difference image between the master and slave images, where this information is directly related to the topographic shape, but still contains elements of deformation, noise, and atmosphere.

The next stage is Differential InSAR Processing, which involves leveling, topography removal and filtering. The method used in the removal of topographic effects is two-pass differential interferometry, with data coming from the interferogram image and the SRTM DEM interferogram. After that, the phase unwrapping stage is carried out to convert images that are still in radian units into metric units, so that information about the amount of deformation can be read properly.

The last step to get the final interferogram is post processing. process leveling process, topography removal, filtering, unwrapping, and geocoding process after that process so that interferogram is georeferenced. Using DEM SRTM 3 to geocode for ensure that the pixel position reflect the position in surface of Earth. This method provide a deeper understanding of the distribution patterns of earthquake damage and ground movement with contributing to disaster mitigation efforts and spatial planning in earthquake-prone areas.

3 Result and Discussion

The Tuban Bawean earthquake was analyzed using the moment tensor method or Mww Phase W. This method provides an overview of the characteristics of the earthquake that occurred, such as the strength of the earthquake, and the depth of the earthquake. The following Table 3 is detailed information about the Tuban Bawean earthquake.

Table 3. Tuban Bawean Earthquake information [10].

Category	Parameter	Value
W-phase Moment Tensor (Mww)	Moment	4.420e+18 N-m
	Magnitude	6.36 Mww
	Depth	11.5 km
	Percent DC	76%
	Half Duration	3.50 s
	Catalog	US
	Data Source	US 2

Category	Parameter	Value
	Contributor	US 2
Nodal Planes	Plane	Strike
	NP1	258°
	NP2	349°
Principal Axes	Axis	Value
	T	4.12E+18
	N	5.52E+17
	P	-4.67E+18

The Okada model, developed by Okada in 1992, is used to calculate the magnitude of plate changes and movements after an earthquake [13]. This model analyzes surface deformation due to seismic activity based on the geometry of the plate fault, which includes important parameters such as dip, strike and slip parameters obtained from the USGS, namely 76°, 258°, and -100° [10].

Based on the results of the Okada model in Figure 3, the earthquake that occurred around Bawean Island had a significant deformation that was centred with a symmetric pattern for the strike slip mechanism, where the dominant movement occurs horizontally due to plate shifts parallel to the fault zone. Although the dominant displacement is horizontal, vertical deformation (uplift and subsidence) often occurs around the fault area. However, strike slip earthquakes usually produce less vertical deformation, but still has a significant impact [16-17].

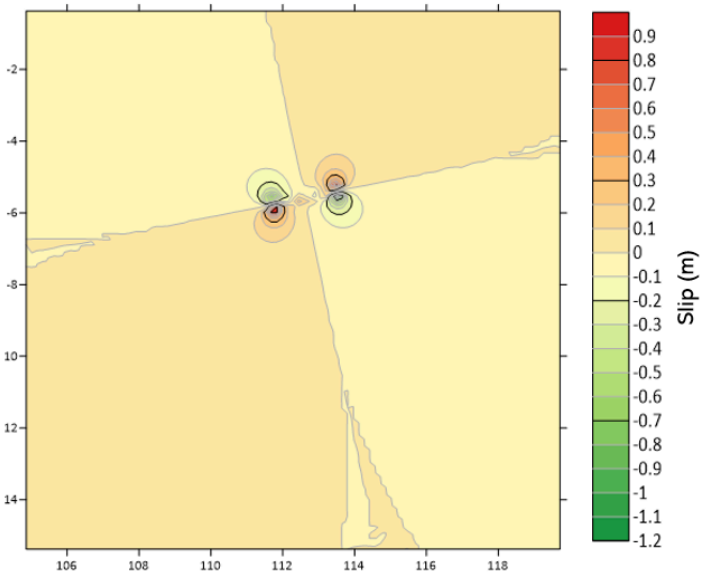

Fig. 3. The vertical movement of the Earth's crust from the M 6.4 Tuban-Bawean earthquake. The earthquake was calculated using the Okada model (1992) and using fault geometry from USGS.

The results of the deformation map are shown in Figure 4, which shows small variations in ground uplift and subsidence. The resulting deformation values range from negative subsidence of about 0.0091 metres to positive uplift of about 0.0069 metres. These relatively small changes in ground elevation are consistent with the

characteristics of strike-slip faults where lateral movement dominates and vertical changes are minimal [16,18].

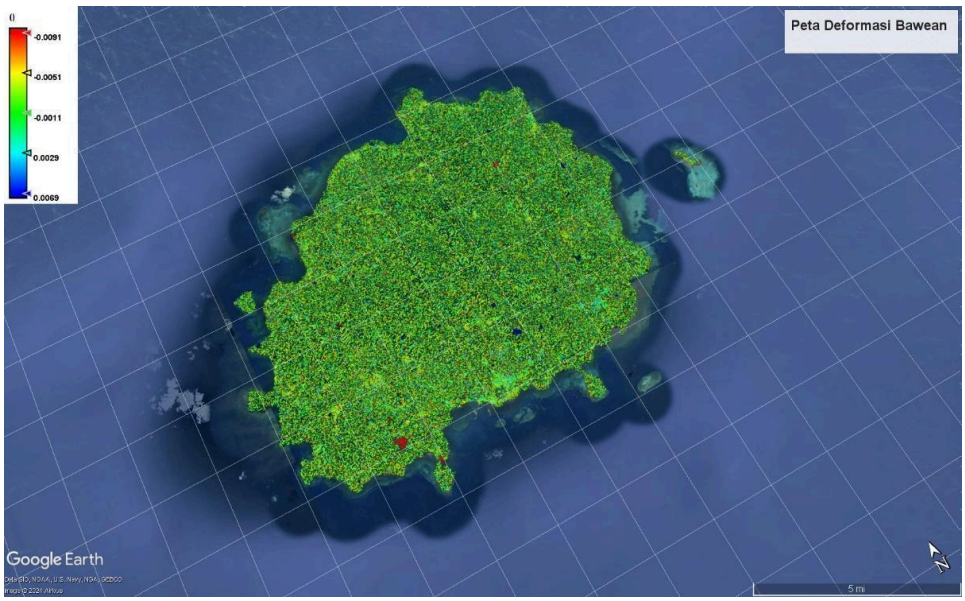

Fig. 4. Deformation map after the M 6.4 Tuban-Bawean earthquake.

The Bawean Island have experience an subsidence or lowering pf the surface when the earthquake that occurred on March 22, 2024 ended. With an average decrease of around 1 mm after the earthquake. The area with alluvial lithology have the most significant subsidence, where the decrease occurred up to 0.0091 meters. Because the area with alluvial lithology contains loose material such as sand, silt, and gravel, this make the areas more susceptible to vertical deformation. When subjected to seismic shocks, the alluvial material tends to experience greater consolidation or compaction [19].

There are other things that have experienced shifts or land movements in several areas on Bawean Island besides land subsiversion even though the number is not much. This increase was detected in the range of 0.0069 meters and occurred in an area dominated by the lithology of kepongan sandstone, which is a Quaternary volcanic rock formation that is different from alluvium with the characteristics of easily compacting. The sandstone formation is denser and tends to uplift due to the elastic response of the rock to seismic pressure.

Critically, these deformation values, although small, highlight that although the Bawean earthquake produced a predominantly horizontal motion pattern, the small vertical components represented by uplift and subsidence can provide clues to the distribution of internal forces acting along the fault [20]. In the context of Bawean's alluvial geology, these effects may become more significant in the long term, particularly in terms of ground response to future earthquakes. Further studies should consider how these small vertical deformations interact with larger lateral faults, and their impact on ground and infrastructure stability in this alluvial-based region.

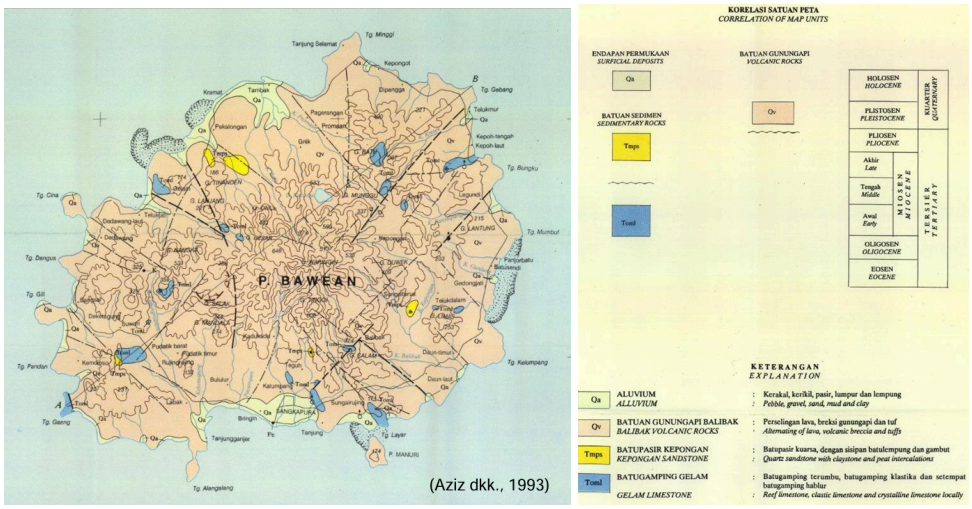

Fig. 5. Geological Map of Bawean Island [21].

The largest deformation that occurred in the Bawean earthquake was in the geological unit in the form of volcanic rock (Qv). This volcanic rock is composed of alternating lava, breccia and tuff [21]. The structure of volcanic rock has the characteristic of high porosity, this causes the volcanic structure to be easily deformed. In addition, this rock is a rock caused by volcanic activity that can leave weak zones such as cracks, so it is more easily deformed than other types of rocks [22]. Qv rocks also have brittle characteristic properties that can cause areas in the Qv rock geology to easily experience deformation or shifting due to tectonic forces. Thus, the magnitude of a deformation also depends greatly on the type of rock and the strength of the rock.

4 Conclusion

The research that has been conducted has resulted in a study using aspects of remote sensing technology and the Okada model. There are important results from this study, namely that overall the analysis shows that the vertical deformation in the form of uplift and subsidence that occurred on Bawean Island was 0.00091 m. The area with this deformation includes coastal areas dominated by alluvial deposits. Meanwhile, the maximum uplift reached 0.006 m with an area that has lithological conditions in the form of volcanic sandstone. The results of the deformation analysis are in line with the Okada model, also showing that the Tuban-Bawean M 6.4 earthquake had a focal mechanism strike slip, where the dominant movement occurs horizontally due to plate movement parallel to the fault zone.

On the other hand, in addition to being relevant for post-earthquake analysis, this study also highlights important implications for earthquake disaster risk management. Based on the identification of areas with alluvial lithology that are prone to vertical deformation, this can be used as a reference for spatial planning. Areas with significant deformation can be prioritised for strengthening earthquake-resistant infrastructure. Analysing the interaction between alluvial lithology and earthquake-induced deformation can provide insight into the

long-term impact of seismic activity on soil and infrastructure stability, which can be used to develop more effective mitigation policies for areas with similar geological risks. Knowledge of deformation-prone areas can also be utilised in public education campaigns aimed at raising public awareness of mitigation measures that can be undertaken independently. Thus, this research can contribute to a more integrated disaster risk reduction effort.

Acknowledgement

This research was supported by funding from the Ministry of Education, Culture, Research and Technology program Scheme KOLABORASI PENELITIAN STRATEGIS (KATALIS) Number 2646/PKS/ITS/2024.

References

1. K. Heki, Ionospheric disturbances related to earthquakes. Ionosphere dynamics and applications, 511–526 (2021)
2. G. Sharma, S. Mohanty, S. Kannaujiya, Ionospheric TEC modelling for earthquake precursors from GNSS data. Quaternary International 462, 65–74 (2017)
3. M. Shah, Earthquake ionospheric and atmospheric anomalies from GNSS TEC and other satellites. Computers in Earth and Environmental Sciences, 387–399 (2022)
4. E. Astafyeva, S. Shalimov, E. Olshanskaya, P. Lognonné, Ionospheric response to earthquakes of different magnitudes: Larger quakes perturb the ionosphere stronger and longer. Geophysical Research Letters 40(9), 1675–1681 (2013)
5. E. Astafyeva, Ionospheric detection of natural hazards. Reviews of Geophysics 57(4), 1265–1288 (2019)
6. G. Savastano, A. Komjathy, O. Verkhoglyadova, A. Mazzoni, M. Crespi, Y. Wei, A. J. Mannucci, Real-time detection of tsunami ionospheric disturbances with a stand-alone GNSS receiver: A preliminary feasibility demonstration. Scientific Reports 7(1), 46607 (2017)
7. B. Corsa, M. Barba-Sevilla, K. Tiampo, C. Meertens, Integration of DInSAR time series and GNSS data for continuous volcanic deformation monitoring and eruption early warning applications. Remote Sensing 14(3), 784 (2022)
8. F. Manta, G. Occhipinti, E. M. Hill, A. Perttu, J. Assink, B. Taisne, Correlation between GNSS‐TEC and eruption magnitude supports the use of ionospheric sensing to complement volcanic hazard assessment. Journal of Geophysical Research: Solid Earth 126(2), e2020JB020726 (2021)
9. B. Hu, J. Chen, X. Zhang, Monitoring the land subsidence area in a coastal urban area with InSAR and GNSS. Sensors 19(14), 3181 (2019)
10. U.S. Geological Survey (USGS), M 6.4 - 110 km N of Paciran, Indonesia. Retrieved from https://earthquake.usgs.gov/earthquakes/eventpage/us6000mkfz/executive
11. M. Scaioni, M. Marsella, M. Crosetto, V. Tornatore, J. Wang, Geodetic and remote-sensing sensors for dam deformation monitoring. Sensors 18, 3682 (2018)
12. M. Liao, J. Dong, M. Ao, L. Zhang, X. Shi, Radar remote sensing for potential landslides detection and deformation monitoring. Natl. Remote Sens. Bull. 25, 332–341 (2021)

13. Y. Okada, Internal deformation due to shear and tensile faults in a half-space. Bull. Seismol. Soc. Am. 82, 1018–1040 (1992)
14. C. Wang, X. Shan, C. Wang, X. Ding, G. Zhang, T. Masterlark, Using finite element and Okada models to invert coseismic slip of the 2008 Mw 7.2 Yutian earthquake, China, from InSAR data. Journal of Seismology 17, 347–360 (2013)
15. A. S. Sunil, M. S. Bagiya, Q. Bletery, D. S. Ramesh, Association of ionospheric signatures to various tectonic parameters during moderate to large magnitude earthquakes: Case study. Journal of Geophysical Research: Space Physics 126(3), e2020JA028709 (2021)
16. E. Astafyeva, L. M. Rolland, A. Sladen, Strike-slip earthquakes can also be detected in the ionosphere. Earth Planet. Sci. Lett. 405, 180–193 (2014)
17. J. F. Dolan, B. D. Haravitch, How well do surface slip measurements track slip at depth in large strike-slip earthquakes? The importance of fault structural maturity in controlling on-fault slip versus off-fault surface deformation. Earth Planet. Sci. Lett. 388, 38–47 (2014)
18. T. P. Dooley, G. Schreurs, Analogue modelling of intraplate strike-slip tectonics: A review and new experimental results. Tectonophysics 574, 1–71 (2012)
19. A. Patria, Earthquake geology of the large left-lateral strike-slip fault system at the Pacific and Australian plate margin, Eastern Indonesia. Ph.D. thesis, Doshisha University (2022)
20. C. Ding, J. J. Dong, M. Le Béon, C. C. Lee, S. K. Ho, S. T. Wang, Characterization of the active fault deformation zone of the Chegualin Fault in the alluvial plain of southwestern Taiwan. Eng. Geol. 342, 107740 (2024)
21. S. Aziz, S. Hardjoprawiro, S. A. Magga, Peta Geologi Lembar Bawean dan Masalembo, Jawa (Pusat Penelitian dan Pengembangan Geologi, Bandung, 1993)
22. H. D. Rachmadhan, J. H. M. Djaya, Volcanic and tectonic interactions in Sangihe Island and Mount Awu: An integrative study in the context of Indonesian geology. J. Geol. Process. Risks Integr. Spat. Model. 1, 39–46 (2023)